

ORBITS AND PHOTOMETRY OF PLUTO'S SATELLITES: CHARON, S/2005 P1, AND S/2005 P2

MARC W. BUIE AND WILLIAM M. GRUNDY

Lowell Observatory, 1400 West Mars Hill Road, Flagstaff, AZ 86001; buie@lowell.edu, grundy@lowell.edu

AND

ELIOT F. YOUNG, LESLIE A. YOUNG, AND S. ALAN STERN

Southwest Research Institute, 1050 Walnut Street, Suite 400, Boulder, CO 80302-5143; efy@boulder.swri.edu, layoung@boulder.swri.edu, alan@boulder.swri.edu

Received 2005 December 19; accepted 2006 March 21

ABSTRACT

We present new astrometry of Pluto's three satellites from images taken of the Pluto system during 2002–2003 with the High Resolution Camera mode of the Advanced Camera for Surveys instrument on the *Hubble Space Telescope*. The observations were designed to produce an albedo map of Pluto, but they also contain images of Charon and the two recently discovered satellites S/2005 P1 and S/2005 P2. Orbits fitted to all three satellites are nearly coplanar and for Charon and P2 have eccentricities consistent with zero. The orbit of the outermost satellite, P1, has a significant eccentricity of 0.0052 ± 0.0011 . Orbital periods of P1, P2, and Charon are 38.2065 ± 0.0014 , 24.8562 ± 0.0013 , and 6.3872304 ± 0.0000011 days, respectively. The total system mass based on Charon's orbit is $(1.4570 \pm 0.0009) \times 10^{22}$ kg. We confirm previous results that orbital periods are close to the ratio of 6:4:1 (P1:P2:Charon), indicative of mean-motion resonances, but our results formally preclude precise integer period ratios. The orbits of P1 and P2, being about the barycenter rather than Pluto, enable us to measure the Charon-to-Pluto mass ratio as 0.1165 ± 0.0055 . This new mass ratio implies a density of 1.65 ± 0.06 g cm⁻³ for Charon (603.6 km radius) and 2.03 ± 0.06 g cm⁻³ for Pluto (1153 km radius), thus adding confirmation that Charon is significantly less dense than Pluto. Finally, by stacking all images we can extract globally averaged photometry. P1 has a mean opposition magnitude of $V = 24.39 \pm 0.09$ and a color of $(B - V) = 0.64 \pm 0.12$. P2 has a mean opposition magnitude of $V = 24.55 \pm 0.10$ and a color of $(B - V) = 0.91 \pm 0.15$.

Key words: astrometry — Kuiper Belt — planets and satellites: individual (Pluto, Charon, S/2005 P1, S/2005 P2)

1. INTRODUCTION

The study of Pluto was greatly facilitated in 1978 with the discovery of its first satellite, Charon (Christy & Harrington 1978). That discovery made possible the accurate determination of the system mass, thus placing the first useful constraints on the mass of Pluto. Later, in the late 1980s, Pluto studies were transformed by the mutual events between Pluto and Charon (e.g., Buie et al. 1992; Binzel & Hubbard 1997; Young et al. 2001). Charon remains an interesting object in its own right, but its role as a tool from which to understand the system should not be understated.

Two new moons were recently discovered in orbit around Pluto (Weaver et al. 2005). More precisely, they orbit the center of mass of the system, which is very close to the Pluto-Charon barycenter. As with Charon, these new objects will be studied in their own right and will also be useful as probes or test masses in the Pluto system. Given astrometry of sufficient precision and time base, one can now easily deduce the precise Charon-to-Pluto mass ratio. One might also hope to determine the masses of the new satellites through their mutual perturbations. However, their mutual gravitational force is more than 3 orders of magnitude weaker than the force exerted on them by Pluto and Charon, possibly masking any measurable effect P1 and P2 may have on each other.

The preliminary orbits computed by Weaver et al. (2005) were based on just two epochs of data separated by only 3 days, much less than a full orbit of either satellite. Also, the data were derived from images in which Pluto and Charon were both saturated. These constraints led to a restricted solution for the orbit, where

it was assumed that the objects were in circular orbits in the same orbital plane as Charon. As we show, these assumptions turned out to be very close to the correct answer.

The data presented in this work are derived from predisccovery observations with the *Hubble Space Telescope* (*HST*) that span multiple orbits of all satellites and do so with images in which Pluto and Charon are not saturated. This paper presents the first unrestricted fits to the orbits of the newly discovered satellites and an improved orbit for Charon.

2. OBSERVATIONS

Images were taken of the Pluto system from 2002 June to 2003 June with the High Resolution Camera (HRC) mode of the Advanced Camera for Surveys (ACS) on the *HST*. The observations were designed to permit construction of a photometrically accurate map of the surface of Pluto. A total of 12 visits were allocated and scheduled to occur at specific sub-Earth longitudes of Pluto at a 30° rotational resolution. The geometric circumstances of the observations are shown in Table 1. Each visit was designed to fit in a single visibility window, but scheduling constraints stretched the time line out beyond a single orbit. Within each visit, two filters were used. The F435W and F555W filters were chosen for their similarity to the standard Johnson *B* and *V* bandpasses, for which there is a substantial heritage of historical data on Pluto. The exposure times were chosen to give comparable signal levels on Charon (a neutrally colored object), but no attempt was made to adjust exposure times based on the light curve from Pluto. The signal level expected in the peak

TABLE 1
CIRCUMSTANCES OF OBSERVATIONS

Midtime (JD)	Visit ID	r (AU)	Δ (AU)	α (deg)	Δt (hr)
2,452,436.846680.....	1	30.518	29.521	0.36	1.71
2,452,440.051972.....	7	30.520	29.527	0.41	1.71
2,452,444.261280.....	3	30.521	29.539	0.50	1.74
2,452,458.083533.....	5	30.526	29.615	0.86	1.65
2,452,472.979577.....	9	30.532	29.751	1.24	1.66
2,452,550.688720.....	11	30.561	30.956	1.71	1.65
2,452,688.548688.....	6	30.613	30.944	1.73	0.70
2,452,750.256191.....	2	30.637	29.983	1.44	1.50
2,452,772.616060.....	8	30.646	29.757	0.91	1.49
2,452,787.606155.....	12	30.651	29.675	0.51	0.70
2,452,789.659917.....	4	30.652	29.668	0.46	1.71
2,452,799.257479.....	10	30.656	29.655	0.32	1.53

NOTES.—Here r and Δ are the heliocentric and geocentric distance to the Pluto-Charon barycenter, respectively, and α is the Sun-barycenter-Earth (phase) angle. The visit ID is a number from the original observation sequence, listed in order of increasing Pluto sub-Earth longitude, and the time span from first to last image in a visit is listed under Δt .

pixel on Pluto was roughly half of the full well of the detector, leaving ample room to accommodate Pluto's light curve without saturating. All F435W exposures were 12 s, and all F555W exposures were 6 s. Peak counts on Pluto ranged from 1900 to 3500 counts, and Charon peak counts were from 700 to 2800 counts. Most of the variations in peak counts are due to variations in sampling of the PSF with an undersampling detector and have little to do with the integrated flux.

During each visit, 16 images were collected in each filter using a customized dither pattern that provided a 4 by 4 subpixel grid superposed on a 1".2 (48 pixel) pattern. This pattern was designed to enable the removal of both large- and small-scale pixelation effects in the image, since the point-spread function (PSF) of the telescope is undersampled by the HRC detector. Distortion corrections are necessary during the processing of the data or the differential distortion in the dither set will lead to a slight blurring of the effective PSF in the co-added images. However, in some visits the new satellites can be seen even without removing the differential distortion, and this crude level of stacking was used for the confirmation referred to in Weaver et al. (2005).

Two other important details about the data set should be noted. First, since the images span a full year, the data were collected at a range of solar phase angles, as well as at various heliocentric and geocentric distances. Second, the data were collected with the largest possible range of roll angle from visit to visit. The first point led to a useful variation in parallax, since the system was viewed from a slightly different orientation during each visit. Unfortunately, the geometry variation also led to a variable signal-to-noise ratio of object images. The second point helped to alleviate potential systematic effects from the geometric distortion and the slightly asymmetric PSF inherent in the camera.

3. ANALYSIS

The new satellites are not directly visible in individual data frames. Note that there are almost 10 stellar magnitudes difference in brightness between Pluto and the faintest satellite. To detect the satellites we had to coregister and co-add the images from a visit. When the data are stacked for each filter separately the objects are visible in many visits in each filter but the signal-to-noise ratios are low. To provide the best possible images for as-

tronometric measurements we chose to co-add all 32 images (both filters) from each orbit into a single image for measurement.

As mentioned earlier and shown in Table 1, the duration of each visit was somewhat variable. The shortest visit did fit in a single visibility window and thus spans only 43 minutes from start to finish. All visits longer than 1 hr were spread over two visibility windows. This time span leads to some smearing of the satellite images depending on how the images are stacked. The upper limit to this smearing is about three HRC pixels for the longest observational time span if Charon is used as a registration point, and both it and the satellite are at minimum separation with respect to Pluto. In practice, the amount of smear is smaller than this and depends on where in its orbit the satellite appears, even when registering on the position of Charon.

The focal plane of ACS is not perpendicular to the optical axis, so a rectangle on the sky looks more like a rhombus in a raw HRC image. In the interest of preserving the maximum sensitivity on these faint objects we chose to implement our own method for removing the geometric distortion from the images by using the forward and inverse distortion coefficients¹ that were available from the Space Telescope Science Institute Web site and documented in Gonzaga et al. (2005).

To rectify the data, each individual image was resampled onto a rectilinear grid. To do this we used the inverse distortion coefficients to map pixel positions in an orthogonal grid back to CCD pixels in the HRC's skewed grid. We defined an undistorted grid with a platescale of 0".025 pixel⁻¹ and a subsampling factor of 8 (virtual platescale of 0".003125 pixel⁻¹). The flux of each subsampled pixel was assigned the value from the distorted image where the position of the subsampled pixel is mapped. In this way the entire image on the subsampled grid is filled from values taken from the original image. Finally, the undistorted, subsampled images were rebinned to the final output platescale by averaging the flux in the 8 by 8 grid mapping to each output pixel.

Once the distortion was removed, the position of Charon was measured using a synthetic photometry aperture of 2.5 pixel radius, and no attempt was made to correct for the variable PSF wing of Pluto at the position of Charon. A test fit was performed on the ACS-based astrometry for Charon to look for effects caused by PSF overlap. If present, the errors should show a double-peaked signature when phased by orbital longitude (maximum error at each minimum separation). This pattern was not seen, and we conclude that the PSF-overlap errors are negligible compared to other sources of error in the astrometry.

The images were then stacked by nearest pixel registration based on Charon's position. Two sets of stacked images were produced. One set was a straight sum of all frames and the other was a robust average (σ -clipping algorithm) meant to suppress cosmic-ray strikes and other image imperfections. In the robust average the cores of Pluto and Charon do not stack properly because of the undersampled PSF and the dithering pattern. The positions of Pluto and Charon were thus measured from the straight sum, and the positions of the faint satellites were measured from the robust average.

All raw positional measurements were made on undistorted frames that are rotated by some angle relative to the sky. We converted all raw measurements to a J2000.0 sky plane measurement by rotating by the angle given in the ORIENTAT key word

¹More information about the reference files can be found at http://www.stsci.edu/hst/acs/analysis/reference_files/idc_tables.html. We used files n7o1634cj_idc.fits and n721640fj_idc.fits for observations made after 2002 October 21 and 2003 March 1, respectively.

TABLE 2
DIFFERENTIAL ASTROMETRY

MIDTIME (JD)	VISIT ID	CHARON		S/2005 P1		S/2005 P2	
		$\Delta\alpha$	$\Delta\delta$	$\Delta\alpha$	$\Delta\delta$	$\Delta\alpha$	$\Delta\delta$
2,452,436.846680.....	1	0.4410	0.1192	-1.5552	0.3647	-0.9313	1.8835
2,452,440.051972.....	7	-0.4501	-0.1106	-1.6298	1.7786	-0.1570	2.1420
2,452,444.261280.....	3	0.4292	-0.6855	-0.7003 ^a	2.8137 ^a	1.0598	0.4708
2,452,458.083533.....	5	0.0046	-0.8393	1.6193	-1.4142	-1.1989	0.1416
2,452,472.979577.....	9	-0.4322	0.6662	-1.3802	-0.5628	1.0678	-1.3731
2,452,550.688720.....	11	-0.0244	0.8020	-1.4565	0.0808	0.4552 ^a	-2.0719 ^a
2,452,688.548688.....	6	-0.2570	-0.5580	1.6226	-1.7965	-0.1714	1.9567
2,452,750.256191.....	2	0.5371	-0.2559	-0.8133	2.8203	0.3261	-2.1782
2,452,772.616060.....	8	-0.5422	0.2580	-0.0662	-2.6896	0.9587	-1.9108
2,452,787.606155.....	12	0.2843	0.5381	-1.0365	2.8517	-0.2195	2.2236
2,452,789.659917.....	4	0.2797	-0.8646	-0.5195	2.8330	0.4735	1.6385
2,452,799.257479.....	10	-0.2771	0.8657	1.6553 ^a	-0.0007 ^a	0.5006	-2.1083

NOTES.—The times for all measurements are the mean of the exposure midtimes for all combined images. All offsets are in units of arcseconds in J2000.0 coordinates relative to the center of Pluto. We adopted uniform astrometric uncertainties of 0".003 for Charon, 0".009 for P1, and 0".015 for P2, chosen to obtain a reduced χ^2 near unity in the orbit fitting.

^a These values were not used in our orbit fits because of anomalously high residuals.

in each image header. This rotation angle is held constant within a visit by the tracking procedure employed by *HST*. In addition, all measurements are treated as relative measurements. The astrometric zero-point reference for each image provided in the image headers is not accurate enough for orbit fitting. However, the positions of all four objects are accurate relative to each other within a frame. Charon was used throughout as a reference point from which the frame-relative measurements were tied together into a single astrometric system.

The quality of the astrometric data is controlled by the quality of the calibrations of the ACS HRC focal plane. The solution for the focal plane distortions includes knowledge of the orientation (relative to ORIENTAT) and image scale to a few parts in 10^{-5} (Anderson & King 2004). Therefore, any systematic errors in the calibration of the focal plane should be negligible for our analysis. The value reported for ORIENTAT has its own uncertainty and is related to the uncertainties in the positions of the guide stars used for pointing and tracking control of *HST*. From past experience we expected the error in ORIENTAT to be about 0".1. However, each visit has its own independent error, since different guide stars were used each time. These errors are present in the astrometry and contribute some small random amount to the overall scatter.

We chose not to use Pluto as a registration object due to its larger and resolved size. Also, Pluto's substantially larger light-curve amplitude relative to Charon (Buie et al. 1997) led us to

use Charon to help minimize errors that might be introduced by center of light-to-center of body offsets.

The positions of Pluto, Charon, P1, and P2 were measured manually in the stacked images. The manual measurement was discretized at 1/10 pixel and done by drawing a 2.5 pixel radius circle on the image. When the circle was judged to be in the correct place based on a highly zoomed image with a logarithmic display stretch, the position was recorded. In the case of Pluto and Charon, the general location is quite obvious, and the manual measurement can attempt to correct for systematic image effects (e.g., overlapping PSFs).

Measuring P1 and P2 was also done with manual centering, but identifying the region of interest is much more important. Analogous to moving object detection for near-Earth object searches or Kuiper Belt surveys, having a geometric constraint enables identification of objects at a much lower signal-to-noise ratio via combining information from multiple epochs. The probability of a chance coincidence across visits that obeys a Keplerian orbit vanishes as the number of visits increases.

A crude predictor was used to identify where to look in the images. The first step was to draw projected ellipses on the image consistent with the discovery information (as found in IAU Circular 8625 [Weaver et al. 2005]). We used their semimajor axes, $a_{P1} = 64,700$ km and $a_{P2} = 49,400$ km, as well as the assumption of coplanar and circular orbits. From this guide we scanned the images for faint objects at any longitude near the

TABLE 3
ORBITAL ELEMENTS FROM UNRESTRICTED FITS (EPOCH = 2,452,600.5)

Orbital Element	Charon	S/2005 P2	S/2005 P1
Period (days).....	6.3872304 (11)	24.8562 (13)	38.2065 (14)
Semimajor axis a (km).....	19571.4 (4.0)	48675 (121)	64780 (88)
Eccentricity e	0.000000 (70)	0.0023 (21)	0.0052 (11)
Inclination i (deg).....	96.145 (14)	96.18 (22)	96.36 (12)
Longitude ascending node Ω (deg).....	223.046 (14)	223.14 (23)	223.173 (86)
Longitude periapsis $\tilde{\omega}$ (deg).....	...	216 (13)	200.1 (3.7)
Mean longitude at epoch L (deg).....	257.946 (13)	123.14 (20)	322.71 (23)

NOTE.—The semimajor axis is measured relative to Pluto for Charon and relative to the Pluto-Charon barycenter for P1 and P2.

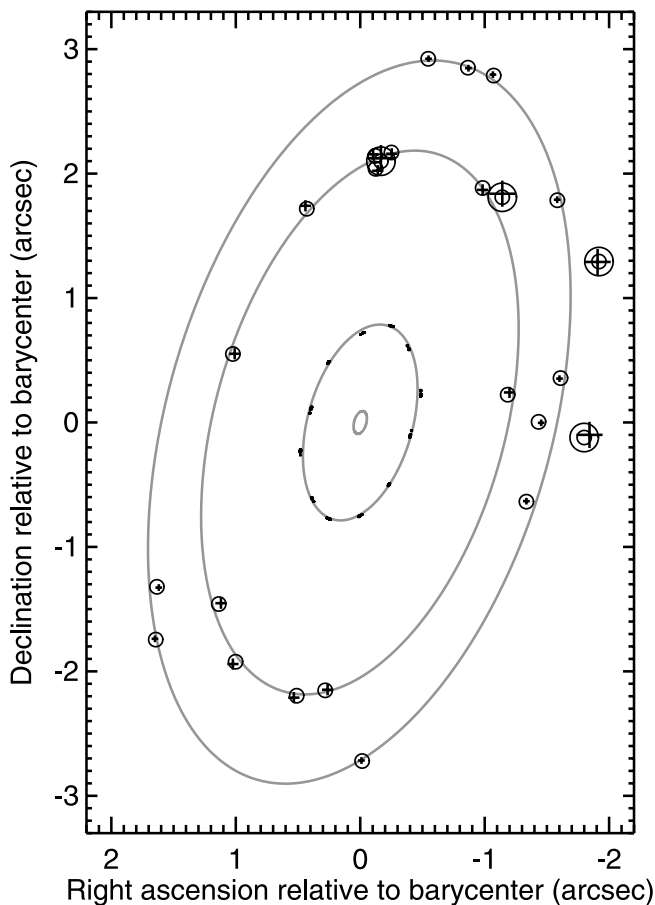


FIG. 1.—Sky plane observations (*points with error bars*) and predicted positions (*open circles*) for P1 and P2, based on our best-fit orbits. Observations of Charon are also shown, but the predicted positions are omitted to avoid clutter. Ellipses show the instantaneous orbits about the barycenter at a single, arbitrary epoch for Pluto, Charon, P2, and P1, from smallest to largest, respectively. The Weaver et al. (2006) measurements are distinguished by double circles for their predicted positions.

projected ellipses of the orbits. Visit 7 showed the most convincing images of objects similar in brightness to that expected for P1 and P2. The reality of the detections was made even more convincing when the F435W and F555W images were stacked separately and the objects appeared in both filters. This detection formed the basis for our confirmation of the existence of P1 and P2 as reported in Weaver et al. (2005, 2006).

Other images also showed possible detections. To check whether these apparent detections were real, we considered whether their longitudes were consistent with possible Keplerian orbits. Starting from the initial orbital periods of the discovery report, we adjusted the periods so as to reproduce the positions of the satellites in visits 1 and 7, arriving at 38.25 days for P1 and 24.85 days for P2. From this information we could crudely predict the locations of the satellites on all frames (stacked relative to Charon) and highlight a 10×10 pixel region of interest on those images. We then located and measured relative to Charon the position of the most convincing source within that region of interest. In all 12 visits a source was identified for P1, and sources were identified for P2 in 8 visits. These measurements, relative to Charon's location, formed the basis for our initial unrestricted orbital fits.

We also needed the position of Pluto, to estimate the location of the barycenter about which the satellites orbit. The centroid positions for Pluto were not used in the orbit-fitting process to

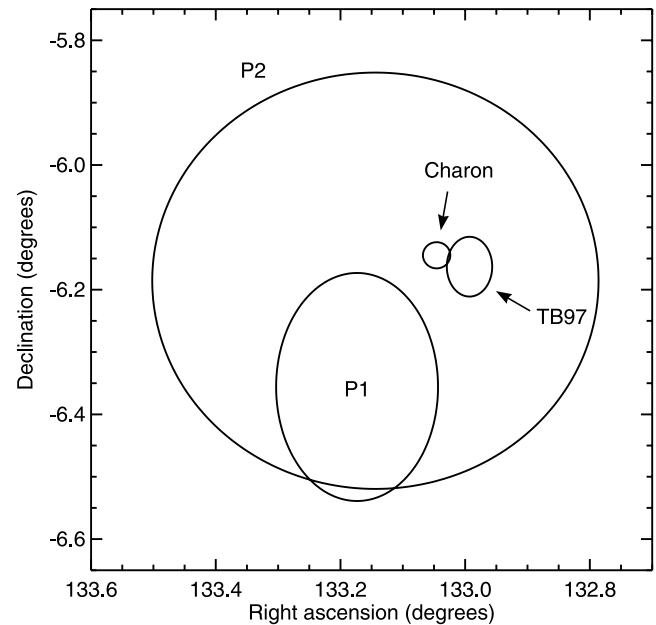


FIG. 2.—The 1σ contours of orbit poles on the J2000.0 sky plane for our best-fit orbits for Charon, P1, and P2, compared with the Tholen & Buie (1997) orbit pole for Charon (marked as “TB97”). These contours were computed from a large set of orbits in which each orbital element is drawn from a Gaussian distribution consistent with the element and its associated uncertainties.

avoid using a center-of-light measurement. However, the primary purpose of this data set was to determine an albedo map for the surface of Pluto (Buie et al. 2005). This map allows for a more precise determination of the center of body during the map-fitting process. A comparison showed a shift of 2–15 mas in right ascension and –10 to 17 mas in declination between the center-of-body position and the center-of-light position. We used the center-of-body location of Pluto relative to Charon in conjunction with the Charon-to-Pluto mass ratio of 0.122 from Olkin et al. (2003) for an initial estimate of the location of the barycenter.

Orbits for P1 and P2 about the Olkin et al. (2003) barycenter were fitted using a downhill simplex minimization scheme (Nelder & Mead 1965), using code developed for fitting orbits of binary transneptunian objects (Noll et al. 2004a, 2004b). Initial results from these fits looked very promising, with residuals mostly at or below a single HRC pixel ($0''.025$). At this step the measurements of P1 from visits 3 and 10 were excluded from the fit due to excessive residuals of 18 and 31 σ , respectively. No image was seen in images stacked relative to Charon for P2 in visits 6, 8, 9, and 11, presumably because the satellite was fainter (with lower signal-to-noise ratio) at larger phase angles and geocentric distances.

We expected that additional detections would be enabled by eliminating the differential smear between Charon and the new satellites. Our initial fitted orbits were used to predict the locations of P1 and P2 relative to Charon. From these positions, offsets were computed enabling us to stack the images on each satellite in turn rather than stacking relative to Charon as was done before. In the resulting P1 and P2 stacked images, we identified sources for the satellites in all 12 visits. This second-generation astrometry went into a second round of unrestricted orbit fits, again relative to the Olkin et al. (2003) barycenter. From the residuals relative to these new orbits it was apparent that one measurement of P2 (visit 11) and two of P1 (visits 3 and 10) still had unacceptably large residuals, and those measurements were removed from further consideration. At this point we had precise

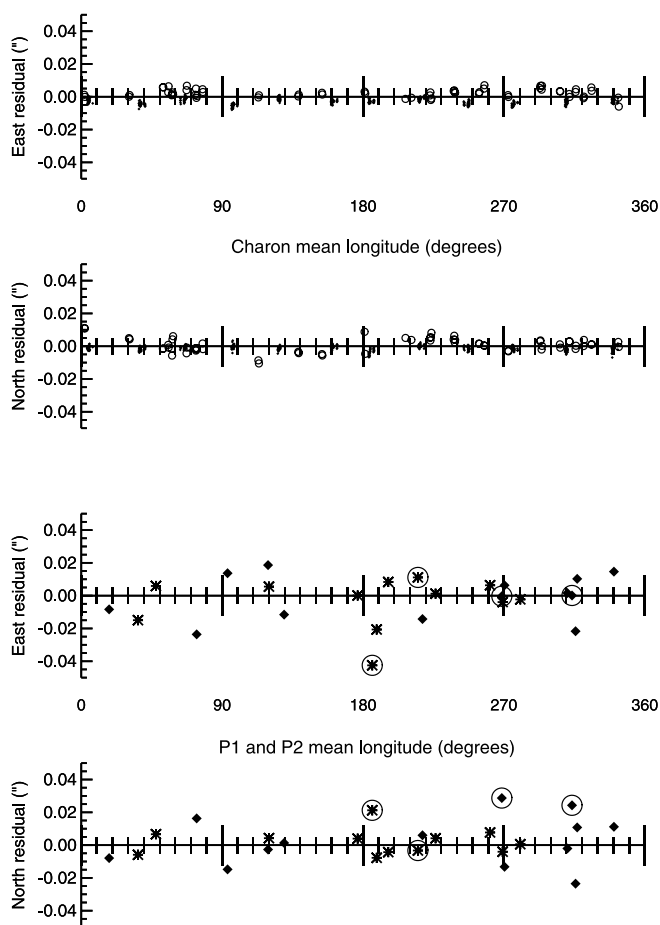


FIG. 3.—East-west and north-south residuals relative to our best-fit orbits plotted vs. orbital longitude. *Top two panels:* Data for Charon. Open circles represent the 60 data points from Tholen & Buie (1997), and diamonds represent our 394 new observations. *Bottom two panels:* Data for P1 (asterisks) and P2 (diamonds), with Weaver et al. (2006) data points circled.

astrometric measurements of Pluto, Charon, P1, and P2 relative to one another. These data are shown in Table 2.

Next we fitted completely unrestricted orbits to the data for Charon, P1, and P2. To extend the time baseline and thus improve the constraint on the orbital periods, we included data from two additional sources. For Charon, 60 positions from Tholen & Buie (1997) were combined with our 394 positions (Charon was measurable in each individual frame, unlike P1 and P2, which could only be measured in the stacked images from each visit). For P1 and P2, our positions were augmented with the two Weaver et al. (2005) positions. In both cases the additional data were collected with different observing strategies and different instruments and thus have different potential systematic issues. For instance, the Tholen & Buie (1997) data were measured relative to the center of light of Pluto, not the center of body. Likewise, the Weaver et al. (2005) positions were measured relative to the center of light of Pluto as deduced from its diffraction spikes, since Pluto itself was severely saturated.

Table 3 summarizes our best-fit orbital elements. Orbital element uncertainties were estimated for each parameter by fixing the parameter in question at a series of values straddling the best value and for each of those values allowing all other parameters to adjust themselves to minimize χ^2 . This process produced a slice through χ^2 space. According to Press et al. (1992), $\chi^2_{\min} + 1$ is the 1σ confidence contour in this space, the location of which

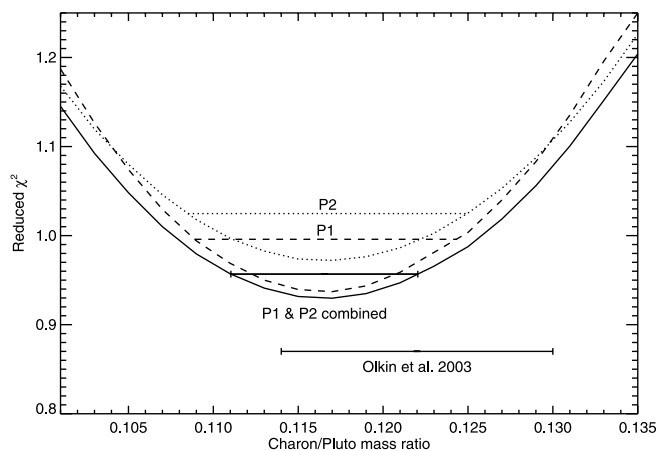


FIG. 4.—Mass ratio slices in reduced χ^2 space for P1 and P2 (dashed and dotted curves, respectively), showing 1σ contours, defined as $\chi^2_{\min} + 1$ (Press et al. 1992). The solid curve represents P1 and P2 combined. The Olkin et al. (2003) mass ratio measurement is also indicated. The fact that reduced χ^2 levels are somewhat below unity suggests that our adopted astrometric uncertainties ($\pm 0''.009$ for P1 and $\pm 0''.015$ for P2) are slightly too conservative.

we report as an uncertainty. In instances of asymmetric χ^2 minima, we conservatively report the uncertainty computed for the shallower sloped side of the valley.

We performed fits restricted to just our new ACS astrometry for all three satellites. The only significant change seen in the orbit fits was larger errors on the periods. However, each orbit fit provides a measurement of the system mass when combining the period and semimajor axis. The fit to the combined data set for Charon gives $M_{\text{total}} = (1.4570 \pm 0.0009) \times 10^{22}$ kg and is the value we adopt for the remainder of this work. The mass inferred from the P1 orbit is $(1.4765 \pm 0.006) \times 10^{22}$ kg, and the mass from the P2 orbit is $(1.480 \pm 0.011) \times 10^{22}$ kg. The P1- and P2-based masses agree with each other but do not completely agree with the Charon-based mass. So far we have been unable to explain this discrepancy, and its resolution is left for future work.

Our new measurement of the semimajor axis of Charon's orbit differs from the measurement of Tholen & Buie (1997). The earlier measurement of $19,636 \pm 8$ km is 65 km (8σ) away from our new value of $19,571 \pm 4$ km. This difference, while apparently significant, is most likely due to the inability to accurately correct for center-of-light versus center-of-body effects in the earlier astrometry. The new data has been corrected for photocenter offsets and should lead to a more robust set of orbital elements.

4. RESULTS

The projected orbits for Pluto, Charon, P1, and P2 are shown in Figure 1. Points with error bars show the sky plane positions of the observations, while the open circles indicate the locations computed from our fitted orbits. The degree to which the circles are centered on the symbols indicates the quality of the fits. One can also see from this figure the effect of the changing geometry through the 12 months of observation and especially for the Weaver et al. (2005) positions obtained 2 yr later. The data (and the fitted orbit positions) do not exactly track the instantaneous apparent ellipse. This figure also shows that we managed to get reasonably complete longitude coverage of both new satellites.

Weaver et al. (2005) noted that the new satellites P1 and P2 orbit near-mean-motion resonances with Charon and with each other. Our improved orbit determinations confirm that the orbital

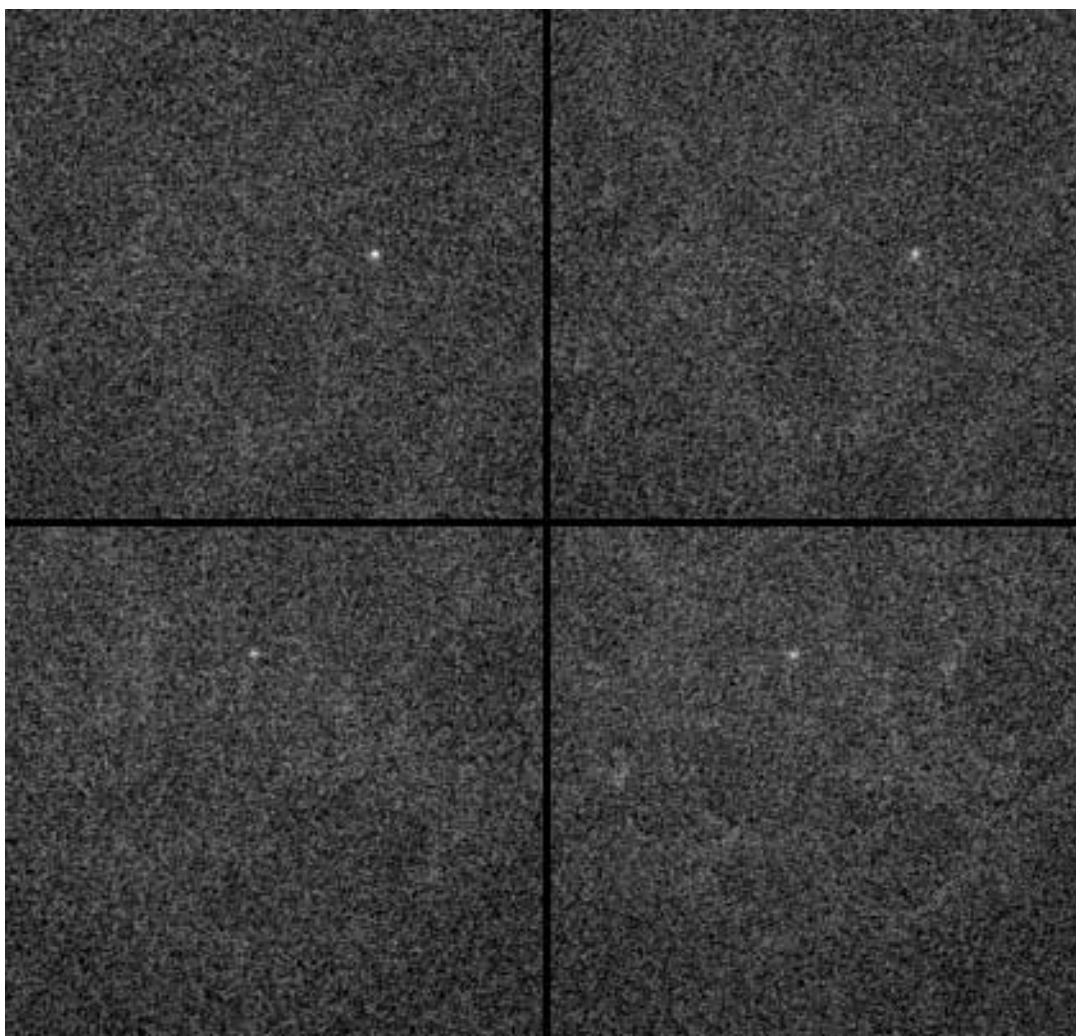


FIG. 5.—Final stacked images for S/2005 P1 and P2. The left panels show the stacked images for the F435W filter. The right panels show the F555W filter data. The top pair of images are stacked based on our fitted ephemeris motion for S/2005 P1, while the bottom pair are stacked on the S/2005 P2 ephemeris. The sky noise per pixel is $0.3 e^- s^{-1}$ and is completely read-noise limited. The peak signals on the satellites in each image are as follows: P1, F435W = $2.93 e^- s^{-1}$; P1, F555W = $2.22 e^- s^{-1}$; P2, F435W = $1.89 e^- s^{-1}$; and P2, F555W = $2.19 e^- s^{-1}$. The display stretch is the same for all four stacked images and is set at -3 to $+10 \sigma$ of the sky level.

periods are indeed near-integer-ratio commensurabilities. However, our uncertainties preclude the precise ratios for simple resonances. Determination of resonant motion will require a full description of the dynamical state of this four-body system using orbital integration calculations. These calculations are beyond the scope of this paper and remain for future work. Nonetheless, if these objects inhabit resonances, the osculating elements would have to vary with time to maintain an oscillating resonant angle. A simple two-body calculation cannot reveal the nature of these mean-motion resonances, nor can it determine the period of oscillations. However, we can use a two-body calculation to determine the time for a resonant argument to circulate by 2π and thus provide a crude upper limit to the timescale for the resonant libration should there be any active resonances.

The orbital period of P1 is 38.2065 ± 0.0014 days, while 6 times the period of Charon is 38.3234 days. This is the period ratio most nearly commensurate, and from the 0.3% difference from a 6 : 1 period ratio we get a circulation of the resonant argument in 2090 ± 80 days, less than 6 yr. Likewise, our period of P2 is 24.8562 ± 0.0013 days, compared with 4 times the period of Charon, which is 25.5489 days. This difference corresponds to a 2.7% difference, and thus, the resonant argument will circulate

in only 229 ± 2 days. Comparing the periods of P1 and P2, we find that their ratio is 1.53710 ± 0.00006 , not the exact ratio of 3/2. Again, circulation would be quite rapid, at just 515 ± 6 days. These circulation periods are all of comparable timescales to the duration of the constraining astrometry for the two-body orbits we have derived. We do not see any obvious periodic deviations from a two-body Keplerian orbit and thus argue that perhaps there are no active resonances.

Eccentricities and inclinations of the satellite orbits will also offer important constraints on possible resonances. The eccentricity of the orbit of P1 (0.0052 ± 0.0011) is significantly non-zero, unlike the orbits of Charon and P2, which are consistent with zero eccentricity. Figure 2 provides our best determination of the orbit poles, showing the 1σ contours for the pole positions for the three satellites, as well as for the Charon orbit determined by Tholen & Buie (1997). The 1σ difference between the two Charon poles may be an artifact of the lack of precise center-of-body measurements for Pluto in the earlier measurements. The same systematic offset can explain the apparently special alignment of the line of apsides in the orbit fitted to the earlier data, as well as the apparent nonzero eccentricity of that orbit.

TABLE 4
PHOTOMETRY

OBJECT	COUNT RATE (photons s ⁻¹)		OBMAG		OPPMAG		APPMAG			DISCOVERY <i>V</i>
	F435W	F555W	F435W	F555W	<i>B_m</i>	<i>V_m</i>	<i>B</i>	<i>V</i>	(<i>B</i> - <i>V</i>)	
Pluto	4748.1 ± 1.5	11136.3 ± 3.2	0.868	...
Charon	1095 ± 0.7	2101.8 ± 1.4	-7.599 ± 0.001	-8.306 ± 0.001	17.259	17.969	16.903	16.193	0.710	...
S/2005 P1	1.64 ± 0.12	2.96 ± 0.24	-0.538 ± 0.081	-1.177 ± 0.089	25.036 ± 0.081	24.393 ± 0.089	23.970 ± 0.081	23.327 ± 0.089	0.64 ± 0.12	22.93 ± 0.12
S/2005 P2	1.20 ± 0.12	2.77 ± 0.24	-0.193 ± 0.110	-1.104 ± 0.095	25.357 ± 0.110	24.546 ± 0.095	24.291 ± 0.110	23.384 ± 0.095	0.91 ± 0.15	23.38 ± 0.17

NOTES.—Uncertainties are based on photon-counting statistics for the object, measured noise in the sky background, and a read noise of 4.7 e⁻. Scaling from instrumental to absolute magnitudes is done using the known mean magnitude for Charon from Buie et al. (1997). Magnitudes for Pluto are not reported due to indeterminate aperture corrections for a resolved object.

We note that every 35.57 days P1, P2, and the barycenter all line up, alternating between P1 and P2 both being on the same side of the barycenter versus being on opposite sides of it. This 35.57 day interval corresponds to one-half of the difference of the mean motion of P1 and P2 and does not require resonances among the satellites. Charon orbits much faster than P1 and P2, so the Charon-Pluto line sweeps across the P1-P2-barycenter line within a few days of each P1-P2-barycenter alignment, providing opportunities when all four objects lie nearly along the same line. Depending on the date of its flyby of the Pluto system, *New Horizons*, NASA's first New Frontiers mission bound for Pluto and the Kuiper Belt (Stern & Cheng 2002), might be able to take advantage of one of these alignments to obtain an especially striking family portrait. The 35.57 day interval is shorter than the period of P1, so the orientation of each successive alignment shifts by about 27° in orbital longitude.

Figure 3 shows details of the residuals from the orbit fits for the *HST* data. The scatter for Charon is quite low in the fits but slightly better for our new data. The mean residual is 3.7 mas, and the maximum residual is 8 mas in our Cycle 11 data. The data from Tholen & Buie (1997) had a mean residual of 5 mas and a maximum residual of 11 mas. The bottom two panels of Figure 3 show the residuals for P1 and P2 on the same scale. The scatter is noticeably higher, owing to the much lower signal-to-noise ratio images, but is still quite respectable, averaging about 9 mas for P1 and 17 mas for P2 (about half of a pixel). The Weaver et al. (2005) residuals (*circled*) are larger on average, owing to the lower spatial resolution of those measurements.

While fitting for each satellite's orbital elements, we also solved for the Charon-to-Pluto mass ratio, which determines the location of the barycenter. Allowing the mass ratio to be a free parameter in these fits resulted in two independent mass ratio estimates, one from the orbit of P1 and one from the orbit of P2. The resulting χ^2 slices, converted to reduced χ^2 by dividing by the number of degrees of freedom, are shown in Figure 4. Our best determination comes from fitting the mass using P1 and P2 orbits simultaneously and results in a mass ratio of 0.1165 ± 0.0055 , consistent with the Olkin et al. (2003) value of 0.122 ± 0.008 . When combined with the new Charon occultation result from Sicardy et al. (2006) of $R = 603.6 \pm 1.4$, we can now determine a much more accurate density for Charon of $1.65 \pm 0.06 \text{ g cm}^{-3}$, where the dominant source of error is the mass ratio. The density of Pluto is thus $2.03 \pm 0.06 \text{ g cm}^{-3}$ assuming a radius² of $1153 \pm 10 \text{ km}$. The radius of Pluto is the dominant source of error and is also the most poorly understood due to the effects of the atmosphere on occultation light curves. Even with the relatively poor knowledge of Pluto's radius, it is clear that Charon is significantly less dense than Pluto.

Each frame recorded insufficient signal from P1 and P2 to permit time-resolved photometry, but some photometric information could be obtained by stacking all 192 images of each filter based on the orbital motion determined previously. The resulting stacked images are displayed in Figure 5. We also stacked images and extracted globally averaged photometry from Pluto and Charon. The total aggregate integration time is 2304 and 1152 s for F435W and F555W, respectively.

Table 4 summarizes the photometric information extracted from the stacked images. Values listed without uncertainties are adopted from Buie et al. (1997). The count rates shown for Pluto are provided as a rough guide to the signal level on the detector. Since Pluto is resolved in these data, our small-aperture fluxes cannot be easily corrected to reliable photometry. However, the aggregate PSF for Charon is nearly identical to that for P1 and P2. "OBMAG" is the instrumental magnitude derived from the count rates using the same convention as Sirianni et al. (2005). This raw photometry was converted to the *UBVRI* system using the transformation coefficients of Sirianni et al. (2005). However, the aperture corrections required a nonstandard method, since the effective PSF was blurred by the stacking process. To correct for the small aperture we assumed that the correction is the same for Charon, P1, and P2. The zero-point correction was determined by using the mean opposition magnitude for Charon from Buie et al. (1997) of $V = 17.259$ and $(B - V) = 0.710$. "OppMag" refers to the transformed photometry that is relative to the mean opposition distance for Pluto's orbit ($r = 39.5 \text{ AU}$, $\Delta = 38.5 \text{ AU}$). Our new photometric data are a peculiar mix of information collected at a range of heliocentric and geocentric distances and solar phase angles. The signal-to-noise ratio in the P1 and P2 photometry is not good enough from single visits to permit the extraction of any light-curve or phase-angle behavior. It is good enough to permit the characterization of globally averaged properties, since the geometries are exactly matched between the three objects.

The "AppMag" columns show the photometry corrected to the circumstances of the discovery of the two satellites as reported in Weaver et al. (2005), their photometry being listed as "Discovery." Our new photometry is in good agreement with the discovery observations to within the uncertainties. The V magnitudes for P1 and P2 are almost identical and correspond to 22 km radii if the satellites' V albedos are similar to Charon's ($\sim 35\%$). The satellites would be larger if their albedos are lower than Charon's: 4% albedos correspond to $\sim 65 \text{ km}$ radii.

The colors presented here indicate that P1 is a spectrally neutral object (solar colors within the uncertainties). This color could indicate a composition similar to Charon. The color for P2 is red like Pluto, but the uncertainty is not particularly constraining. Both satellites exhibit colors that are common in the Kuiper Belt (e.g., Peixinho et al. 2004). The photometric observations here are not of sufficient quality to place tight constraints on surface properties, and such work remains for future studies. Recent observations reported in IAU Circulars 8676 and 8686 (Mutchler et al. [2006] and Stern et al. [2006], respectively) include new measurements of colors and provide additional astrometry on the new satellites. The new astrometry reported agrees with our orbit solution to better than 30 mas. The new colors were shown to be neutral for both objects, but additional observations will be required to make full sense of these objects.

5. CONCLUSIONS

The major conclusions of this paper are as follows: (1) The orbits of P1 and P2 are very nearly circular, with eccentricities of 0.0052 ± 0.001 and 0.0023 ± 0.0021 , respectively. (2) The orbits of P1 and P2 are nearly coplanar with Charon's orbit, with the pole positions offset from Charon's orbit pole by $0^\circ 25' \pm 0^\circ 11'$ and $0^\circ 10' \pm 0^\circ 33'$, respectively. (3) The orbit periods of P1 and P2 are within a few percent of integer multiples of Charon's period but differ significantly from exact integer multiples, with periods 3.89155 ± 0.00020 and 5.98170 ± 0.00022 times Charon's orbit period, respectively. (4) We find redder color for P2 than P1,

² Choosing a value for the radius of Pluto is not a simple matter. Current measurements from mutual events and stellar occultations do not completely agree, and explanations of the differences depend on the models chosen to interpret the data. Here we use the number adopted in most Pluto map-fitting projects with an error bar chosen to include the range of model values for the radius from mutual event and stellar occultation data.

$(B - V) = 0.91 \pm 0.15$ versus 0.64 ± 0.12 , but this difference may not be significant (1.4σ). (5) We have improved measurements for the mass of Pluto + Charon at $(1.4570 \pm 0.0009) \times 10^{22}$ kg and a better determination of the Charon-to-Pluto mass ratio of 0.1165 ± 0.0055 . The discovery of P1 and P2 allow us to measure the position of the barycenter relative to bodies in the Pluto system. Compared to the previous method of measuring the barycentric motion relative to field stars, these measurements should be much less susceptible to systematic errors.

The orbit in this work is already good enough for the *New Horizons* spacecraft to image P1 with MVIC (the widest field of view camera) at its closest approach ($\sim 73,000$ km). However, the spacecraft gets much closer to P2 (closest approach $\sim 21,000$ km), and our orbit is not good enough for close approach targeting with any camera. Looking ahead to both the

New Horizons flyby and the possibility of stellar occultation opportunities, it will be important to continue to observe these new satellites. Their orbits are quite good already but need to be refined further to enable future in-depth observations.

This work was supported by grant HST-GO-09391.01 from the Space Telescope Science Institute (STScI). These results would not have been possible without the expert assistance of the late Andy Lubenow (STScI). Thanks to D. Tholen for numerous constructive suggestions. We also thank the free and open source software communities for empowering us with many of the tools used to complete this project, notably, Linux, the GNU tools, LaTeX, and FVWM.

REFERENCES

- Anderson, J., & King, I. R. 2004, StSCI Instrument Science Report ACS 2004-15 (Baltimore: STScI), <http://www.stsci.edu/hst/acs/documents/isrs/isr0415.pdf>
- Binzel, R. P., & Hubbard, W. B. 1997, in *Pluto and Charon*, ed. S. A. Stern & D. J. Tholen (Tucson: Univ. Arizona Press), 85
- Buie, M. W., Grundy, W. M., Young, E. F., Young, L. A., & Stern, S. A. 2005, *BAAS*, 37, 4903
- Buie, M. W., Tholen, D. J., & Horne, K. 1992, *Icarus*, 97, 211
- Buie, M. W., Tholen, D. J., & Wasserman, L. H. 1997, *Icarus*, 125, 233
- Christy, J. W., & Harrington, R. S. 1978, *AJ*, 83, 1005
- Gonzaga, S., et al. 2005, ACS Instrument Handbook, Version 6.0 (Baltimore: STScI), <http://www.stsci.edu/hst/acs/documents/handbooks/cycle15/cover.html>
- Mutchler, M. J., et al. 2006, *IAU Circ.*, 8676, 1
- Nelder, J., & Mead, R. 1965, *Comput. J.*, 7, 308
- Noll, K. S., Stephens, D. C., Grundy, W. M., & Griffin, I. 2004a, *Icarus*, 172, 402
- Noll, K. S., Stephens, D. C., Grundy, W. M., Osip, D. J., & Griffin, I. 2004b, *AJ*, 128, 2547
- Olkin, C. B., Wasserman, L. H., & Franz, O. G. 2003, *Icarus*, 164, 254
- Peixinho, N., Boehnhardt, H., Belskaya, I., Doressoundiram, A., Barucci, M. A., & Delsanti, A. 2004, *Icarus*, 170, 153
- Press, W. H., et al. 1992, *Numerical Recipes in C: The Art of Scientific Computing* (New York: Cambridge Univ. Press)
- Sicardy, B., et al. 2006, *Nature*, 439, 52
- Sirianni, M., et al. 2005, *PASP*, 117, 1049
- Stern, S. A., & Cheng, A. 2002, *Eos*, 83, 384
- Stern, S. A., et al. 2006, *IAU Circ.*, 8686, 1
- Tholen, D. J., & Buie, M. W. 1997, *Icarus*, 125, 245
- Weaver, H. A., et al. 2005, *IAU Circ.*, 8625, 1
- . 2006, *Nature*, 439, 943
- Young, E. F., Binzel, R. P., & Crane, K. 2001, *AJ*, 121, 552